Velocity Measurements Near the Empennage of a Small-Scale Helicopter Model

Susan Althoff Gorton
Army JRPO-AFDD

James F. Meyers
Fluid Mechanics
and Acoustics Division

John D. Berry
Army JRPO-AFDD

Langley Research Center
Hampton, VA

Summary

A test program was conducted in the NASA Langley 14- by 22-Foot Subsonic Tunnel to measure the flow near the empennage of a small-scale powered helicopter model with an operating tail fan. Three-component velocity profiles were measured with Laser Velocimetry (LV) one chord forward of the horizontal tail for four advance ratios to evaluate the effect of the rotor wake impingement on the horizontal tail angle of attack. These velocity data indicate the horizontal tail can experience unsteady downwash angle variations of over 30° due to the rotor wake influence. The horizontal tail is most affected by the rotor wake above advance ratios of 0.10. Velocity measurements of the flow on the inlet side of the fan were made for a low-speed flight condition using both conventional LV techniques and a promising, non-intrusive, global, three-component velocity measurement technique called Doppler Global Velocimetry (DGV). The velocity data show an accelerated flow near the fan duct, and vorticity calculations track the passage of main rotor wake vortices through the measurement plane. DGV shows promise as an evolving tool for rotor flowfield diagnostics.

Introduction

As rotor and fuselage designs become more integrated, compact, and complex, close rotor-wake-fuselage interactions and interference are an increasingly important part of the performance characteristics of rotorcraft. Reference 1 attributes the importance of interactional effects for modern helicopters to increased disk loading, more compact designs, low level flight requirements, and the increased requirement for directional trim after the loss of the tail rotor which results in larger vertical tail surfaces. These effects are especially important in the design and placement of the anti-torque system and the hortizontal and vertical stabilizers as documented in References 2-3.

Much work has already been done experimentally and analytically to define the interaction effects between the rotor and the fuselage (Refs. 4-15). More limited is the amount of experimental data available for analyzing the main rotor/anti-torque interactions (Refs. 16-22). As advanced configurations such as the RAH-66 are designed and manufactured with sophisticated and new anti-torque devices, there is a need for high-quality experimental data to support the development of more flexible analytical models capable of treating these types of configurations (Refs. 23 and 24). Reference 25 specifically cites the difficulty in predicting unsteady empennage loads at speeds below 40 knots. While Reference 26 provides experimental pressure data at model scale for a generic T-tail empennage, and Reference 27 discusses the tremendous amount of testing involved in the Light Helicopter (LH) design process, there does not appear to be specific information in the literature on the velocities in the flowfield near an operating tail fan.

In order to investigate the rotor wake /fuselage /empennage interactions near the empennage of a powered small-scale helicopter with an operating tail fan and a T-tail, the U. S. Army Joint Research Program Office, Aeroflightdynamics Directorate, in cooperation with the NASA Langley Measurement Sciences and Technology Branch, recently conducted a wind tunnel test program in the 14- by 22-Foot Subsonic Tunnel. Velocity data were acquired forward of the horizontal tail for four flight conditions, documenting the unsteady downwash near the horizontal tail. Velocity data were also obtained on the inlet side of the fan for one flight condition, providing information about the inflow into the tail fan. Pressure data obtained on the fuselage during a different phase of this same test program are already being used for CFD code validation (Ref. 28).

Presented at the American Helicopter 52nd Annual Forum, Washington, D.C., June 4-6, 1996.

Model and Instrumentation

The test program was conducted in the Langley 14- by 22-Foot Subsonic Tunnel using the Army's 2-Meter Rotor Test System (2MRTS) with a four-bladed, 15-percent scale rotor, a fuselage model representative of the RAH-66, and the tunnel's three-component Laser Velocimetry (LV) system. In addition, a new optical flow measurement technique, Doppler Global Velocimetry (DGV), was applied for the first time to a rotorcraft flowfield during this test program.

The 14- by 22-Foot Subsonic Tunnel is a closed-circuit, atmospheric wind tunnel designed for the low-speed testing of powered and high-lift configurations (Ref. 29). In the open test section configuration, the walls and ceiling are lifted out of the flow, leaving a solid floor under the model. In this configuration, the tunnel can achieve a maximum dynamic pressure of about 92 lb/ft^2. This investigation was conducted with the tunnel in the open test section configuration to allow complete optical access to the rotor flowfield. For this test program, the test section floor was lowered two feet to install the LV optics. A false floor with a window, flush with the rest of the tunnel, was placed over the optics

Figure 1 shows the 2MRTS ready for testing in the tunnel. The LV system is also visible in the photograph. The rotor system which was installed on the 2MRTS had a 4-bladed, articulated hub with blades that closely matched the planform, twist, and airfoils of the RAH-66 blades. No attempt was made to dynamically scale these blades. Because the only hub available for testing was a 4-bladed hub, there were some deviations from scale from an actual model of the 5-bladed RAH-66. The radius of the blades when installed on the 4-bladed hub was reduced by one inch from a true 15-percent scale RAH-66. In addition, the use of only four blades reduced the rotor solidity and resulted in higher blade loads for any given thrust coefficient. The blades and hub are described in more detail in Table 1.

The fuselage was a 15-percent scale model of the RAH-66 and was instrumented with over 200 pressure ports and 4 unsteady pressure gages. Forces and moments on the rotor and fuselage were measured separately by two six-component, strain gage balances. As mentioned earlier, some pressure data can be found in Reference 28. The fuselage is shown in detail in Figure 2.

The anti-torque device of the configuration was modeled by an air-powered, tip-driven, 8 in diameter, 22-bladed fan mounted in the tail fan duct. The fan configuration is shown in Figure 3. As can be seen in the photograph, the fan duct section was painted black to minimize the optical reflections from the surface.

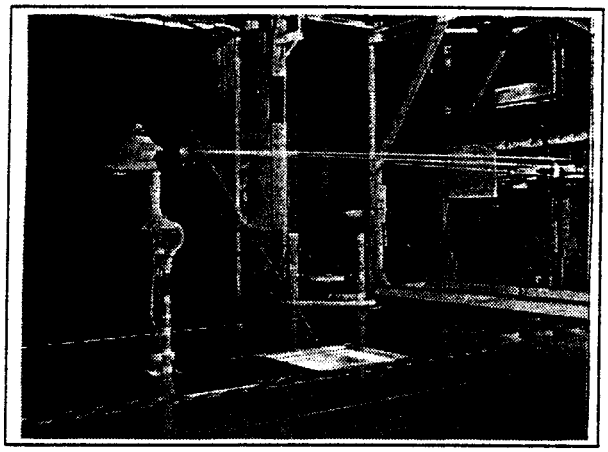

Figure 1. Model and LV system installed in tunnel.

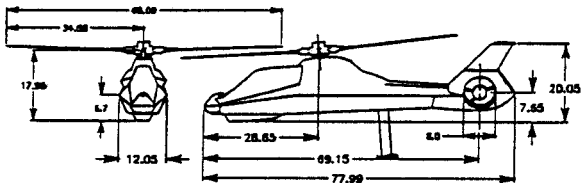

Figure 2. Description of fuselage. All dimensions in inches.

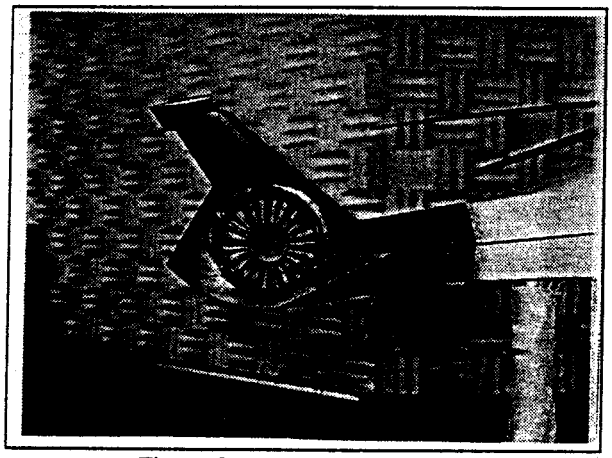

Figure 3. Tail fan configuration.

LV System

The LV system was a three-component system operating in the backscatter mode. Most components of the system are described in References 30-31; this paper presents the first data obtained with the upgraded three-component system. The streamwise and vertical components of velocity are measured by optics located on

the side of the tunnel, out of the flow; the lateral crossflow component of velocity is measured by optics which are located beneath the tunnel floor. The traversing mechanisms of the three components are computer-controlled to ensure the sample volumes of the three sets of beams are positioned at a single location. As can be seen in Figure 1, the third component beams originating beneath the floor were angled at 33° to the vertical. This angle was necessary to optically access the inflow area of the tail fan due to the cant of the tail fan duct. Corrections for this rotation in the lateral velocity component were applied to the data during post-processing.

Except for its long focal length and zoom lens assembly, the system was a standard fringe-based LV system; polystyrene particles (1.7 micron) suspended in an alcohol and water mixture were used to seed the flow. The velocity data were acquired using Frequency Domain Processors (FDP's) to maximize the signal to noise ratio of the data. The LV data acquisition system was designed to allow acquisition of rotor azimuth position in addition to the velocity measurements so that an "azimuthal history" of the velocity could be reconstructed in post-processing.

DGV System

DGV is a fairly new technique to measure three-component velocity data that has been demonstrated mainly for application to fixed-wing studies (Ref. 32). At this point in time, only steady-state data have been acquired with the technique; however, the extension of DGV to capture the unsteady rotor flowfield is under development at Langley. As a first step in applying DGV to rotorcraft, the technique was used during this test program to measure three-component mean (or steady-state) velocity near the fan tail. The use of DGV during this test program established the feasibility of using DGV in the facility for the relatively low-speed and reversed flows that occur in rotor wakes.

The DGV system which was used was based on the theoretical development described in References 32-34. For this test program, three sets of two cameras each were used; each camera pair measured a component of velocity. Each camera pair consisted of a signal camera and a reference camera, as shown in Figure 4. Although the camera pairs did not measure orthogonal velocity components, post-test processing transformed the velocity measurements into the standard u, v, and w components.

A light sheet produced by a single frequency Argon-ion laser was projected into the flow, as shown in Figure 5. This sheet defined the measurement plane for the three-component DGV velocity measurements. The DGV measurements were made in the same plane as the LV measurements so that detailed comparisons of the two techniques could be made. Propylene glycol smoke was injected into the flow from the settling chamber of the tunnel. As the smoke passed through the light sheet, it scattered light that was Doppler-shifted in optical frequency proportional to the particle velocity.

Figure 4. DGV signal and reference camera pair.

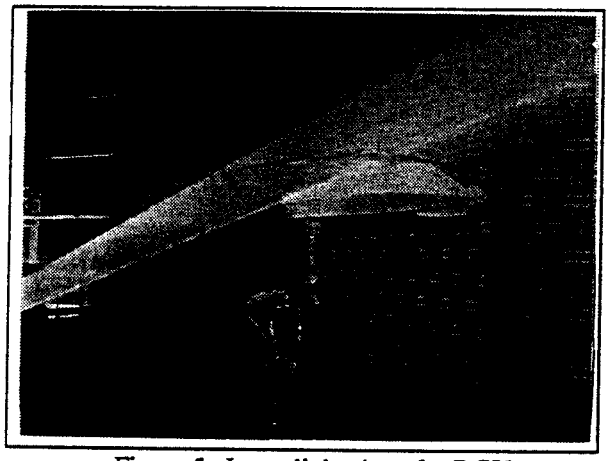

Figure 5. Laser light sheet for DGV.

At each camera pair location, an iodine vapor cell was placed in front of the signal video camera to attenuate the collected scattered light in proportion to the shift in the laser light optical frequency. The reference camera, without an iodine cell, was used to provide a reference image of the scattered light intensity distribution emitted by the smoke passing through the light sheet. Normalization of the signal image by this reference image removed spatial variations in light intensity caused by differences in smoke density, particle size distributions, and nonuniformities in the light sheet. The resulting image amplitude distribution was processed to

yield a map of the velocity flowfield in the locations illuminated by the laser light sheet.

Measurement Locations and Test Procedures

The measurement locations are described briefly below and are shown in Figure 6. The operating conditions for each configuration are documented in Table 2.

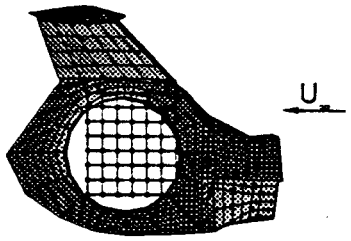

(a) Side view of fan measurement locations

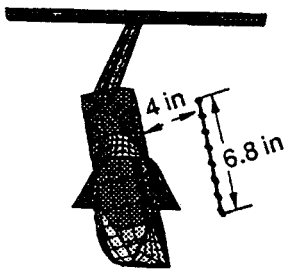

(b) Rear view of fan measurement locations.

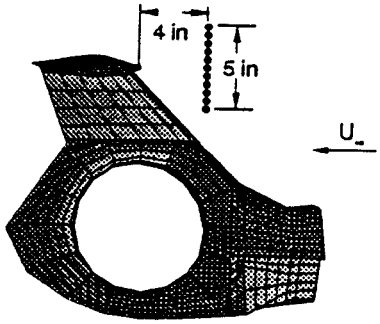

(c) Side view of horizontal tail measurement locations.

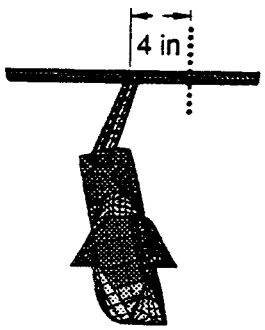

(d) Rear view of horizontal tail measurement locations.

Figure 6. Velocity measurement locations.

Horizontal Tail

LV data were obtained for ten points in a vertical line one chord forward and one chord to the right of center of the hortizontal tail with both the main rotor and tail fan operating (MRTF) for advance ratios of 0.05, 0.07, 0.10, and 0.15. The rotor thrust coefficient was 0.007, and the rotor shaft angle was held at a constant -0.65°.

Tail Fan

In order to investigate non-linear interference effects between the main rotor wake and the tail fan, velocity data were acquired on the inlet side of the tail fan for several combinations of unpowered and powered main rotor and tail fan conditions.

Baseline LV and DGV data were acquired for a baseline reference condition (BL), which consisted of only the fuselage (no main rotor installed) and the tail fan covered with plates to prevent flow through the tail duct. This established the reference flow conditions at the measurement plane due to just the presence of the fuselage in the freestream. The tunnel speed was 55 ft/sec, which was the speed for a main rotor advance ratio of 0.07 if the main rotor had been installed and operating. The velocity was measured with LV in three locations near the covered tail fan. At each location, the velocity was very close to the freestream value, indicating little interference due to the fuselage alone at these locations.

TF For the tail fan operating alone condition (TF), the main rotor was not installed, and the tail fan was operated at an rpm which was known to generate about 340 in-pounds of anti-torque. This was the amount of anti-torque which was predicted before the test program to be required to trim the configuration in yaw. The tunnel speed was again set to 55 ft/sec. Measurements of velocity with the LV were made at a limited number of locations as reflections from the tail fan spinner and the

duct made the measurements difficult to acquire with the backscatter system. DGV data were acquired for the entire measurement plane.

MR LV and DGV measurements were obtained in the same measurement plane for the main rotor operating alone condition (MR). This configuration had the main rotor installed and operating, and the tail fan was uncovered but free-wheeling. The tail fan was allowed to free-wheel to minimize the optical reflections. As the fuselage yawing moment did not vary greatly between this configuration and the BL configuration, it was not expected that this change from covered fan to free-wheeling fan would affect the data comparisons. The operating conditions were a main rotor advance ratio of 0.07, a thrust coefficient of 0.005, and a shaft angle of -0.65°. The main rotor was trimmed to zero first harmonic flapping. Due to the relatively small size of the model and the low thrust coefficient, the calculated wall effects corrections were insignificant, and no wall corrections were applied to these data. Measurements of the rotor torque averaged 330 in-pounds, indicating the TF anti-torque setting was very close to that required for trimming the system for the MR configuration. Measurements of velocity were made with LV at more locations near the tail fan for this configuration as it was assumed that the rotor wake would cause more non-uniform distribution of velocity than either the BL or the TF configuration.

MRTF The final configuration was for both the main rotor and tail fan operating (MRTF). In this configuration, the main rotor was trimmed in the same manner as for the MR configuration with the advance ratio = 0.07, the thrust coefficient = 0.005, and the shaft angle = -0.65°. The tail fan was operated at the same rpm and pressure as for the TF configuration. However, although the fan rpm was approximately the same as for the TF configuration, the anti-torque was 640 in-pounds, almost twice as much as needed to trim the model to zero yawing moment. This increased performance by the tail fan appears to be due to the interference effects between the rotor wake and the tail fan. It was noted during the test program that this operating condition appeared unstable in yaw which indicated the fan was experiencing some type of inlet stall phenomenon. The main concentration of LV measurements were for this MRTF configuration. Again, DGV meausurements were acquired for the entire plane for this configuration.

Data Acquisition and Reduction

LV

The LV data acquisition process consisted of placing the sample volume at the measurement location and acquiring data for a period of nine minutes or until 4096 velocity measurements were made in each of the longitudinal, vertical, or lateral components of velocity. The LV measurements were not made in coincidence, which would have required that each component of velocity be measured at the same time from the same particle. Instead, the flow was assumed to be periodic with rotor blade passage, and each component was allowed to be measured individually; this dramatically reduced the time required to obtain the LV data. During this process, as was mentioned earlier, conditional sampling techniques were employed to associate each measured velocity with the azimuth of the rotor blades at the time when the measurement was made. At the conclusion of the process, the measurement location was changed, and the acquisition process was repeated.

For each measurement location, the raw data were reviewed, and the histograms of the velocities in each of the three components were processed to improve the signal-to-noise ratio. The data were "binned" into 2.8° azimuthal increments, and the mean velocity for the location was calculated from the mean of all the azimuth bins. Since the data were associated with a rotor position, it was possible to sort the data by azimuthal position, thereby reconstructing a time history of velocity at each measurement location which represented one average rotor revolution.

The largest contributors to the uncertainty in the LV measurements are the measurement of the crossbeam angle and the particle lag. The LV system error for the velocity measurements in this paper is estimated at 1.3% velocity.

DGV

Since the DGV system used a continuous wave laser light sheet, synchronization to the rotor azimuth was not possible, and the measurements averaged the velocity field over 1/60 second. Therefore, the DGV velocity data were mean data, averaged over several rotor revolutions. For each test condition, 100 frames of data were acquired from the cameras, and each frame took approximately 20 sec to acquire. The DGV system was essentially a pixel by pixel sensor, with each pixel containing independent information about the flow. In the post-processing, for a pixel to be considered to contain valid data, there had to be smoke in that pixel from all three camera components. Therefore, in the final averaged frame of data, some of the pixels had more averages than others; the maximum

number of averages possible in this investigation was 100.

Combining the velocity images from the three DGV camera sets yielded the standard u, v, and w component velocity fields. Appropriate image warping techniques to remove optical and perspective distortions were applied to the images during the processing. The usual processing calibrations for any image data which include pixel calibration, background light removal, dewarping corrections, and intensity calibrations were also applied to the data. During the post-test processing of the DGV data, it was discovered that the temperature regulators for each of the three iodine vapor cells allowed the temperature of the cells to fluctuate during the data acquisition. Although a temperature variation was noted during the test program, the application of insulation around the iodine vapor cell (as seen in Fig. 4) was thought to have eliminated the problem. However, the fluctuations were significant enough to require a correction to the data in the post-test processing. This correction increases the uncertaintly in the DGV measurements by as much as 5 ft/sec. The total uncertainty in the DGV measurement system for this test program has not yet been quantified.

Discussion of Results

Horizontal Tail Velocity Measurements

The average downwash angle, as measured from the horizontal using LV one chord forward of the hortizontal tail, is shown in Figure 7 for several advance ratios. In each of these cases, both the main rotor and the tail fan are operating at the conditions indicated in Table 2. As expected, the downwash angle decreases with increasing advance ratio. Similarly, the average sidewash angle is shown in Figure 8.

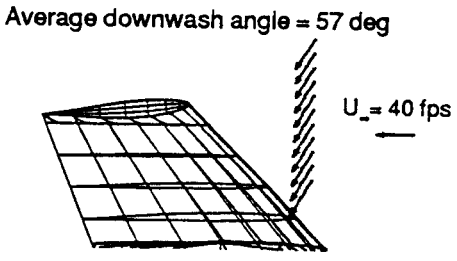

(a) $\mu = 0.05$.

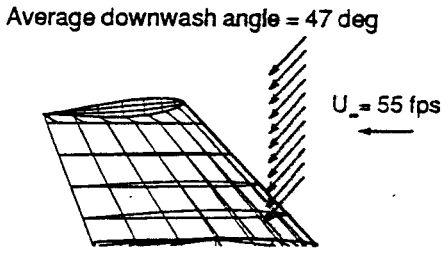

(b) $\mu = 0.07$.

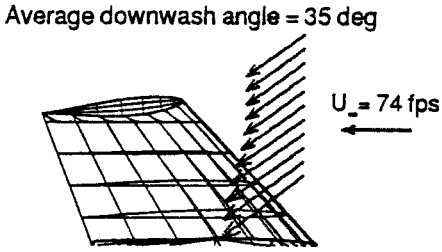

(c) $\mu = 0.10$.

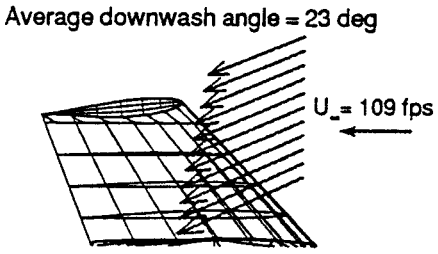

(d) $\mu = 0.15$

Figure 7. Average downwash angle forward of the horizontal tail for MRTF.

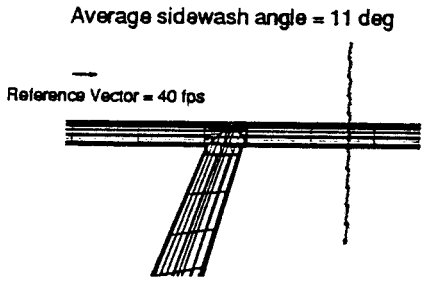

(a) $\mu = 0.05$.

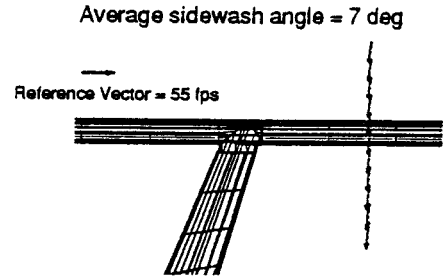

(b) $\mu = 0.07$.

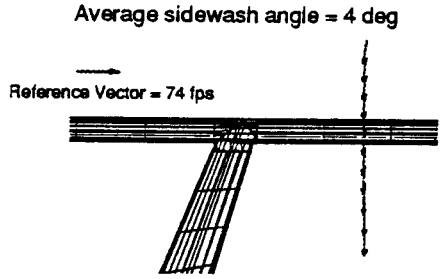

(c) $\mu = 0.10$.

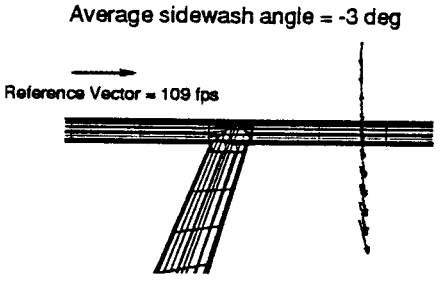

(d) $\mu = 0.15$.

Figure 8. Average sidewash angle forward of the horizontal tail for MRTF.

Large variations in the unsteady downwash and sidewash angles were also measured using the LV system. Typical plots of the unsteady flow angles calculated from the unsteady velocity data are shown in Figure 9 for a height one-half inch below the horizontal tail for each of the advance ratios tested. The results indicate over 30 degrees of unsteady fluctuation are encountered near the horizontal tail at the blade passage frequency with the most unsteadiness occurring at an advance ratio of 0.10. Carpet plots of the unsteady angles for all the advance ratios which were tested are presented in Figure 10. These plots show the variation in unsteady angle with height above the tail section at each advance ratio.

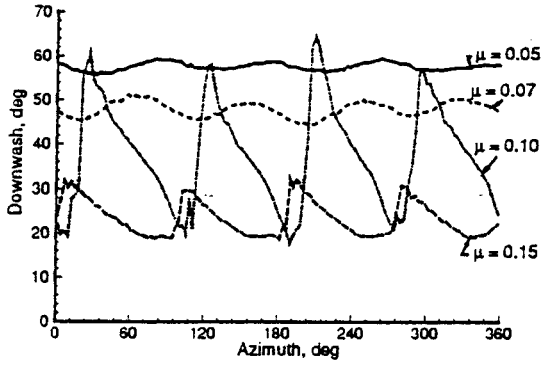

(a) Downwash angle.

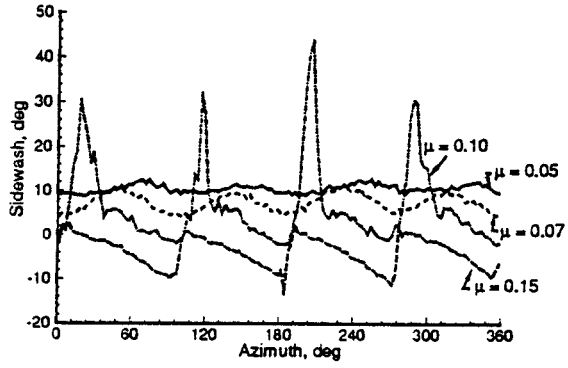

(b) Sidewash angle.

Figure 9. Unsteady angles for a location 0.5 in below the horizontal tail.

From the unsteady data, a determination of the position of the rotor wake relative to the horizontal tail can be made by analyzing the 4/rev RMS content of the velocity. A strong 4/rev content indicates that the rotor wake is the dominant flow feature. Figure 11 summarizes the position of the rotor wake relative to the horizontal tail for the advance ratios tested, showing the tail immersed in the wake above advance ratios of 0.10. These results generally agree with those in Reference 26, considering the different geometry and flight conditions of the two test programs.

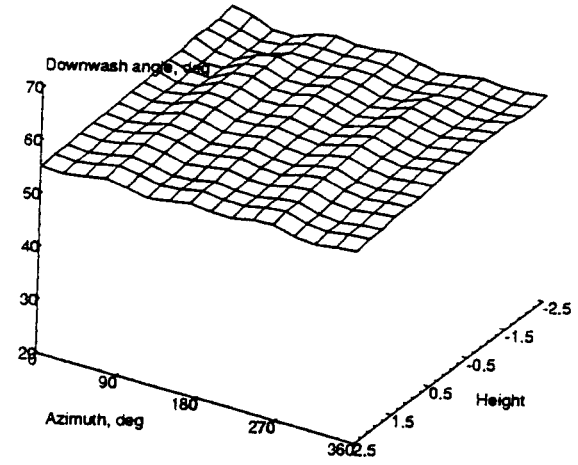

(a) $\mu = 0.05$.

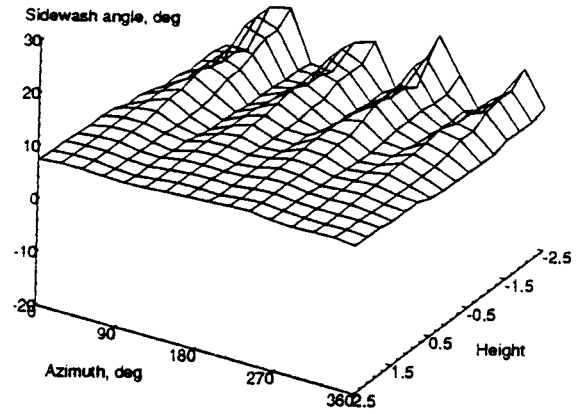

(b) Concluded.

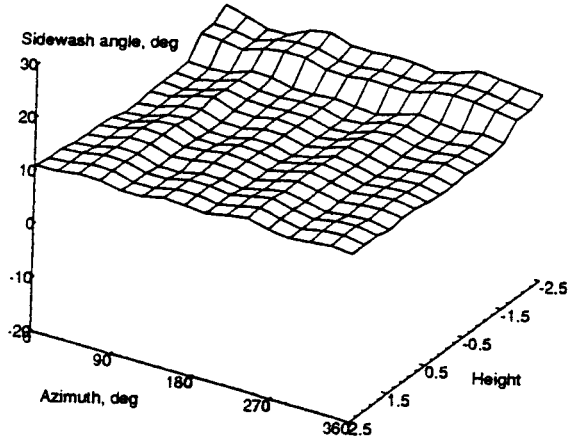

(a) Concluded.

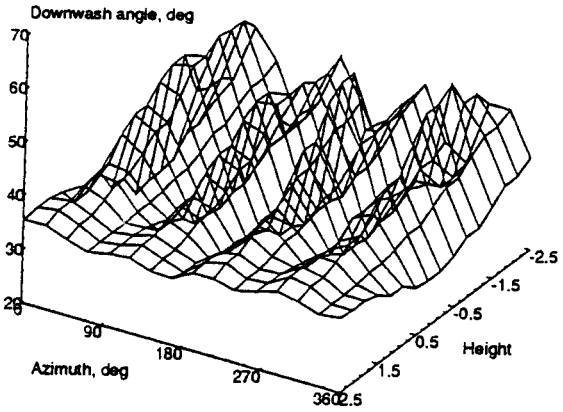

(c) $\mu = 0.010$.

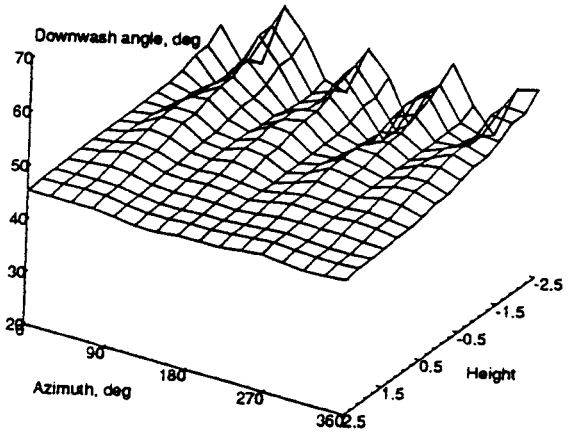

(b) $\mu = 0.07$.

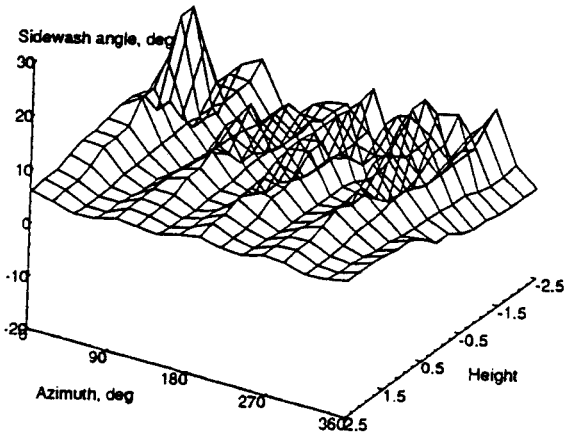

(c) Concluded.

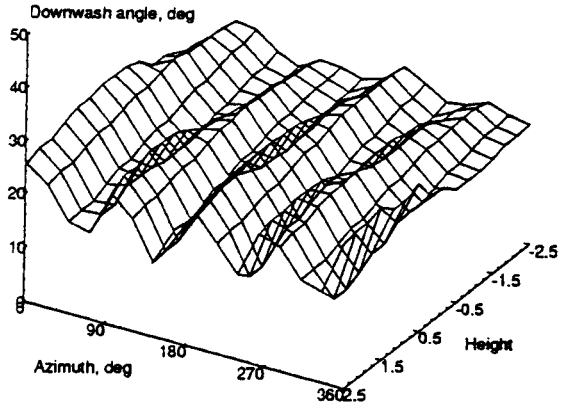

(d) $\mu = 0.15$.

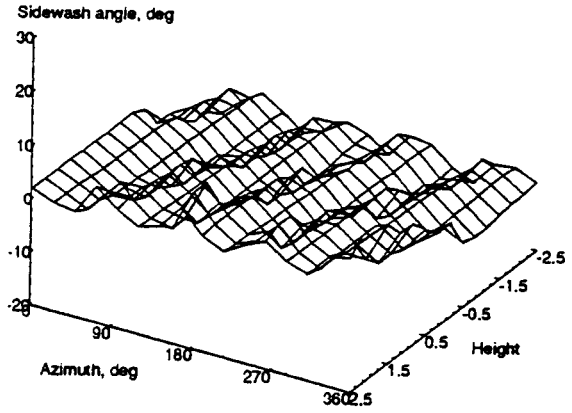

(d) Concluded.

Figure 10. Unsteady downwash and sidewash angles for MRTF.

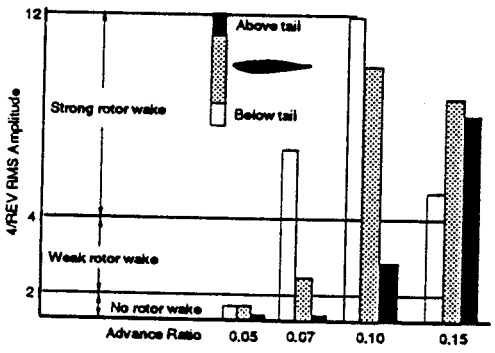

Figure 11. Unsteady wake impingement at horizontal tail for MRTF.

Figure 12 illustrates an interesting feature of the unsteady flow near the horizontal tail. At an advance ratio of 0.15, a significant 2/rev content becomes present in the flow. At the lower advance ratios of the test program (represented by the sample plot in Fig. 12a), this is not present. Reference 26 also reports a strong 8/rev in the flow near the horizontal tail; the data in the present investigation show periodic content at several multiples of the 4/rev frequency, as well as frequencies between the multiples of the 4/rev.

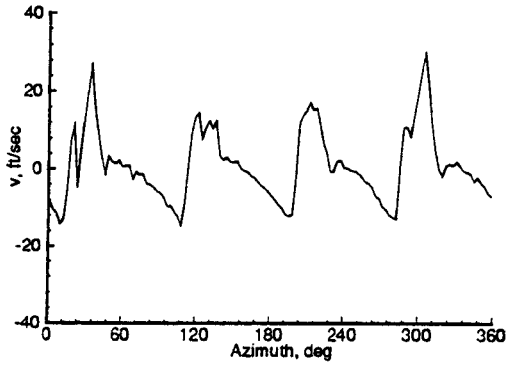

(a) $\mu = 0.10$.

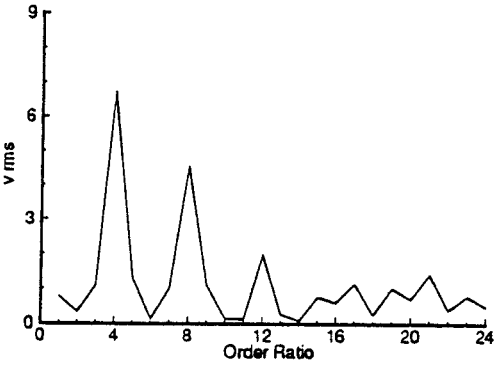

(a) Concluded.

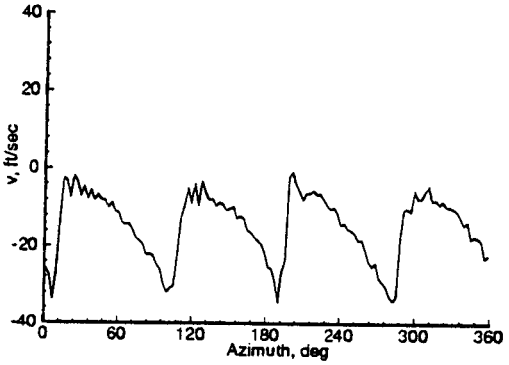

(b) $\mu = 0.15$.

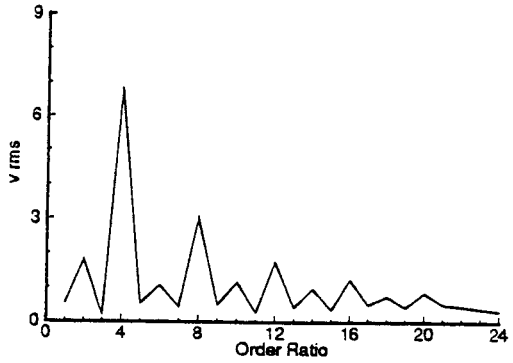

(b) Concluded.

Figure 12. Velocity and order ratio analysis for location 2 inches below centerline of horizontal tail, MRTF.

Tail Fan Velocity Measurements

Figure 13 presents contour plots in the fan system coordinates of the average streamwise velocity, u, the normal (perpendicular to the fan) velocity, v, and the vertical (parallel to the fan) velocity, w. These are presented for the MRTF configuration operating at the conditions listed in Table 2. Note the accelerated flow at the forward section of the duct. The photographs in Figure 14 show surface flow visualization of the empennage for one of the runs. The flow visualization, supported by the velocity data, indicate the flow is separated along the upstream lip of the tail fan duct. The photographs also show a large region of separation on the aft part of the empennage. There are also several separation lines on the vertical tail and the junction between the vertical tail and the tail fan duct. This occurs on both the right and left hand side of the empennage.

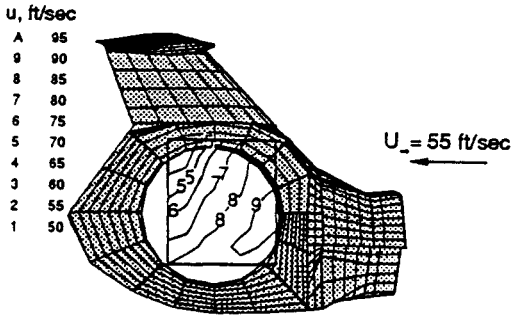

(a) Streamwise velocity, u.

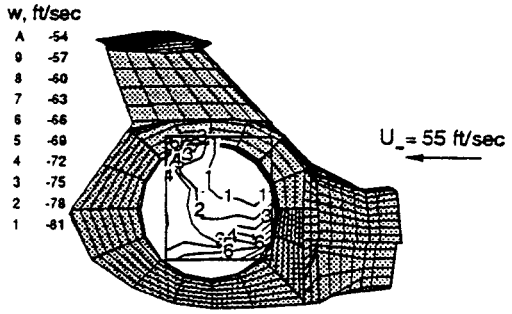

(b) Vertical velocity, w.

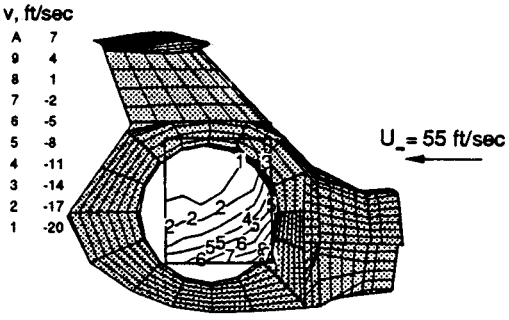

(c) Normal velocity (inflow), v. (Corrected)

Figure 13. Contour plots of LV average velocity data for MRTF configuration.

(a) Inlet side of tail fan.

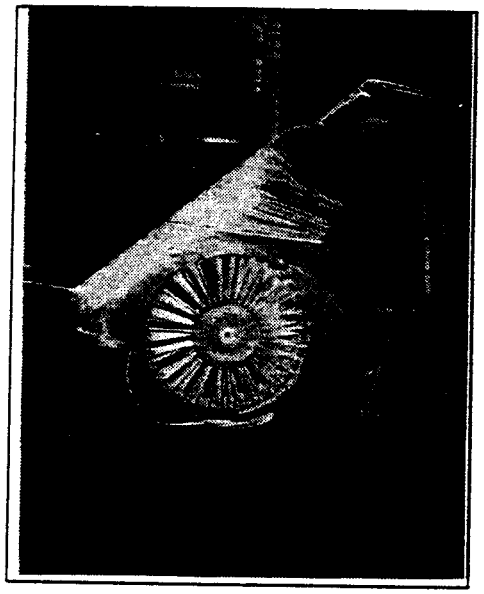

(b) Outflow side of tail fan.

Figure 14. Surface flow visualization of empennage for $\mu = 0.07$ and thrust coefficient of 0.005, MRTF configuration.

In Figure 15, the DGV data are presented as velocity maps for the MRTF configuration. In each of these maps, the speed of the flow is represented by the level of the gray scale. The data in Figure 15 are for the individual components of velocity in the wind tunnel coordinate system (i.e., not rotated into the fan coordinate system). These plots illustrate how DGV maps the entire velocity field illuminated by the smoke in the light sheet. The dark areas on the right-hand side of the figures are the absence of smoke in the laser sheet.

As these velocity maps are difficult to assess, especially in gray scale, Figure 16 presents the DGV data for a single slice horizontally through the measurements for each velocity component. The location for this slice of a single row of pixels is shown on Figure 15 by arrows on each of the velocity maps. The LV data for the same configuration are also presented on the plots in Figure 16. Note that the DGV data provide a tremendous increase in the resolution of the velocity measurement locations; there are over 400 DGV measurements to compare to 7 LV measurements in the same horizontal line.

Although the DGV data do not match exactly with the LV data, there is enough similarity to encourage the continued development of the global velocity technique. The DGV technique requires some additional refinement and improvements before it is established as a reliable, accurate tool for rotorcraft; however, the immense potential payoff of increased efficiency in flowfield measurement capability is worth the investment.

(a) Velocity map for u-component.

(b) Velocity map for v-component.

(c) Velocity map for w-component.

Figure 15. DGV data for MRTF configuration, wind tunnel coordinates.

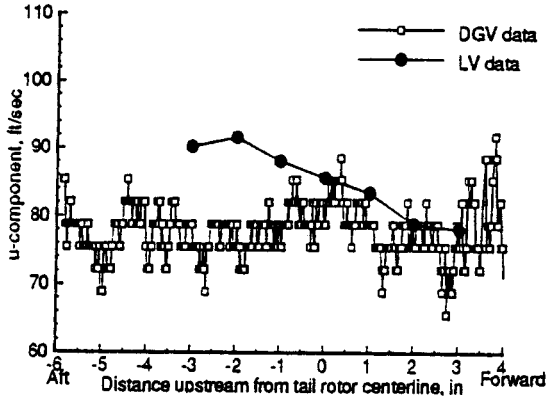

(a) Streamwise component, u.

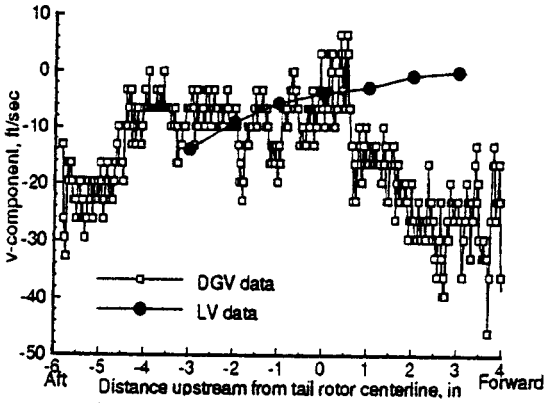

(b) Normal (inflow) component, v.

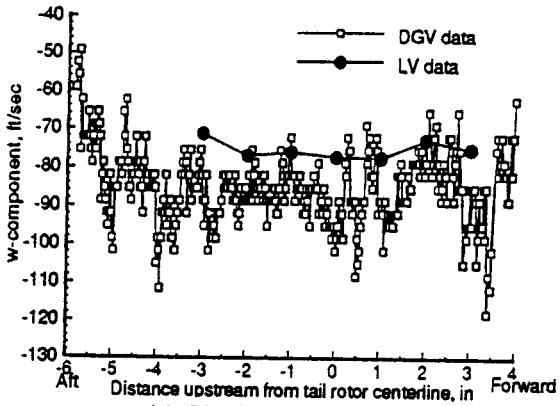

(c) Vertical component, w.

Figure 16. Comparison of DGVand LV data for MRTF configuration, wind tunnel coordinates.

The purpose of acquiring data for several different model configurations was to allow the determination of the non-linear interference effects between the main rotor wake and the tail fan flow. This was determined by subtracting the combination of the MR and TF velocities from the MRTF velocities. The results for four locations in the measurement plane are given in Table 3. There are limited results for this part of the investigation due to the small number of measurements made for the TF configuration. From a percentage standpoint, the non-linear effects are most significant in the normal velocity (v) component, which is influenced the greatest by the tail fan flow.

For each measurement location, the unsteady, azimuthally-dependent velocity was measured by LV in each velocity component. For a given azimuth, the velocity at each measurement point can be extracted and plotted on a contour plot to give an effective velocity "snapshot" of the entire measurement grid. As these data were processed at azimuth intervals of 2.8°, there are 128 snapshots of velocity in each of the three components. These data can be obtained electronically by contacting the author.

From each snapshot of velocity, the vorticity component perpendicular to the measurement grid plane was calculated for the MRTF configuration. By examining each azimuthal "snapshot", it became evident that areas of concentrated vorticity were convecting through the measurement plane. Figure 17 shows examples of two azimuth angles. Both positive (into the plane) and negative vorticity are present in the plots. The phenomenon occurs 4 times per revolution, and the convection velocities, on average, were calculated to be 45 ft/sec in the downstream direction and 52 ft/sec in the vertical direction. This equates to a skew angle of 41°. Using the equation in Reference 35, the classical wake skew angle is calculated to be 42°. This very close agreement indicates that the vorticity seen in the data is evidence of the main rotor blade wake vortices passing through the measurement plane at the blade passage frequency.

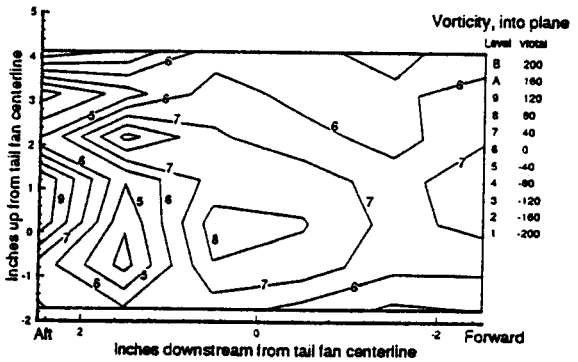

(a) Azimuth = 150 degrees.

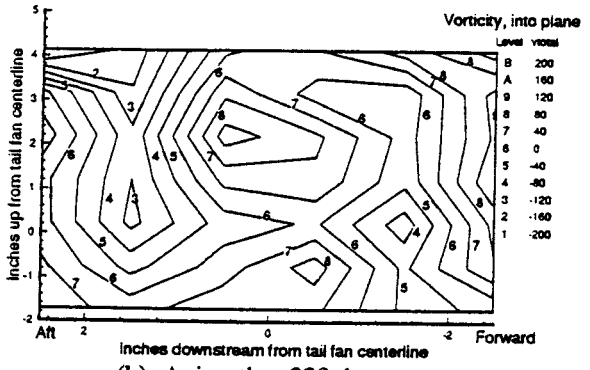

(b) Azimuth = 220 degrees.

Figure 16. Vorticity contours calculated from unsteady LV data for MRTF configuration.

Conclusions

In order to investigate the rotor wake /fuselage /empennage interactions near the empennage of a powered small-scale helicopter with an operating tail fan and a T-tail, the U. S. Army Joint Research Program Office, Aeroflightdynamics Directorate, in cooperation with the NASA Langley Measurement Sciences and Technology Branch, recently conducted a wind tunnel test program in the 14- by 22-Foot Subsonic Tunnel. Velocity data were acquired forward of the horizontal tail for four flight conditions, documenting the unsteady downwash near the horizontal tail. Velocity data were also obtained on the inlet side of the fan for one flight condition, providing information about the inflow into the tail fan. The major conclusions from this study are:

1. The horizontal tail surface experiences large changes (over 30°) in the unsteady sidewash and downwash angles due to the influence of the rotor wake. The horizontal tail is most affected by the rotor wake above advance ratios of 0.10.

2. There is an accelerated flow pattern near the operating fan tail, and flow visualization indicates the flow is separated on part of the forward duct lip as well as at the base of the vertical tail for an advance ratio of 0.07 and a main rotor thrust coefficient of 0.005.

3. Main rotor wake vortices are seen to convect through the LV measurement plane with approximately the same skew angle as predicted by classical theory.

4. A new flow measurement technique, Doppler Global Velocimetry, shows promise for making global velocity measurements.

Acknowledgements

The authors wish to thank Angelo Cavone, Deane Reis, Mark Fletcher, Todd Hodges, Judy Jumper, Joe Lee, Derry Mace, Dan Neuhart, and Richard Schwartz for their assistance in completing this program.

References

1. Sheridan, P. F., and Smith, R. P., "Interactional Aerodynamics--A New Challenge to Helicopter Technology," American Helicopter Society 35th Annual Forum, Washington, DC, May 1979.

2. Roesch P., and Vuillet, A., "New Designs for Improved Aerodynamic Stability on Recent Aerospatiale Helicopters," American Helicopter Society 37th Annual Forum, New Orleans, May 1981.

3. Prouty, R. W., and Amer, K. B., "The YAH-64 Empennage and Tail Rotor--A Technical History," American Helicopter Society 38th Annual Forum, Anaheim, May 1982.

4. Ahmed, S. R.; Raddatz, J.; and Hoffman, W., "Analysis of Helicopter Rotor-Fuselage Interference with Time Averaged Pressure Distribution," 17th European Rotorcraft Forum, Berlin, 1991.

5. Ahmed, S. R.; and Meyer, F. W., "A Mach-Scaled Powered Model For Rotor-Fuselage Interactional Aerodynamics And Flight Mechanics Investigations," American Helicopter Society International Specialists' Meeting on Rotorcraft Basic Research, Atlanta, GA, 1991.

6. Bettschart, N.; Hanotel, R.; Ilbas, D.; and Desopper, A., "Theoretical And Experimental Studies Of Helicopter Rotor/Fuselage Interaction," ONERA TP 1991-198, 1991.

7. Norman, T. R.; and Yamauchi, G. K., "Full-Scale Investigation Of Aerodynamic Interactions Between A Rotor And Fuselage," American Helicopter Society 47th Annual Forum, Phoenix, AZ, 1991.

8. Berry, J. D., "RWF Rotor-Wake-Fuselage Code Software Reference Guide," NASA TM 104078, July, 1991.

9. Leishman J. G.; and Bi, N. P., "Measurements Of A Rotor Flowfield And The Effects On A Fuselage In Forward Flight," 16th European Rotorcraft Forum," Glasgow, 1990.

10. Lorber, P. F.; and Egolf, T. A., "An Unsteady Helicopter Rotor-Fuselage Aerodynamic Interaction Analysis," *Journal of the American Helicopter Society*, Vol. 35, (3), July 1990.

11. Meyer, F. W., "The Influence Of Interactional Aerodynamics Of Rotor-Fuselage-Interference On The Fuselage Flow," *Vertica*, Vol. 14, (2), 1990.
12. Dehondt, A.; and Toulmay, F., "Influence Of Fuselage On Rotor Inflow Performance And Trim," *Vertica*, Vol. 14, (4), 1990.
13. Wilson, F. T., "Fuselage Aerodynamic Design Issues And Rotor/Fuselage Interactional Acrodynamics. Part 1: Practical Design Issues," AGARD, Aerodynamics of Rotorcraft, N91-18048, 1991.
14. Rand, O.; and Gessow, A., "Model For Investigation Of Helicopter Fuselage Influence On Rotor Flowfields," *Journal of Aircraft*, Vol. 26, May 1989.
15. Trept, T., "A 0.15-Scale Study Of Configuration Effects On The Aerodynamic Interaction Between Main Rotor And Fuselage," NASA CR-166577, Jan. 1984.
16. Huber, H., and Polz, G., "Studies on Blade-to-Blade and Rotor-Fuselage-Tail Interferences," In AGARD Prediction of Aerodynamic Loads on Rotorcraft, N83-17470-08-01, 1983.
17. Fitzgerald, J., and Kohlhepp, F., "Research Investigation Of Helicopter Main Rotor/Tail Rotor Interaction Noise," NASA CR-4143, May, 1988.
18. Jacobs, E. W., Fitzgerald, J. M., and Shenoy, R. K., "Acoustic Characteristics Of Tail Rotors And The Effects Of Empennage Interactions," American Helicopter Society 43rd Annual Forum, St. Louis, MO, 1987.
19. Balch, D. T., "Experimental Study Of Main Rotor Tip Geometry And Tail Rotor Interactions In Hover," NASA CR 177336, Feb. 1985.
20. Balch, D. T., Saccullo, A., and Sheehy, T. W., "Experimental Study Of Main Rotor/Tail Rotor/Airframe Interactions In Hover," NASA CR-166485, June, 1983.
21. Edwards, B. D., Peryea, M. A., and Brieger, J. T., "0.15 Scale Model Studies Of Main And Tail Rotor Interaction," American Helicopter Society National Specialists' Meeting on Aerodynamics and Aeroacoustics, Arlington, TX, 1987.
22. Martin, R. M., Burley, C. L., and Elliott, J. W., "Acoustic Test Of A Model Rotor And Tail Rotor: Results For The Isolated Rotor And Combined Configuration," NASA TM 101550, Feb. 1989.
23. Pagnano, G., and Saporiti, A., "Current European Research Activities In Helicopter Interactional Aerodynamics," 17th European Rotorcraft Forum, Berlin, September 1991, Paper 91-35.
24. Philippe, J., "ONERA Makes Progress In Rotor Aerodynamics, Aeroelasticity, And Acoustics," *Vertiflite*, Sept/Oct. 1992, pp. 48-53.
25. Torok, M. S., and Ream, D. T., "Investigation of Empennage Airloads Induced by a Helicopter Main Rotor Wake," American Helicopter Society 49th Annual Forum, St. Louis, May 1993.
26. Moedersheim, E., and Leishman, J. G., "Investigation of Aerodynamic Interactions Between a Rotor and a T-Tail Empennage," Presented at the American Helicopter Society Aeromechanics Specialist Meeting, Fairfield County, CT, October 1995.
27. Keys, C., Sheffler, M., Weiner, S., and Heminway, R., "LH Wind Tunnel Testing: Key to Advanced Aerodynamic Design," American Helicopter Society 47th Annual Forum, Phoenix, May 1991.
28. Duque, E. P. N., Berry, J. D., Budge, A. M., and Dimanlig, A. C. B., "A Comparison of Computed and Experimental Flowfields of the RAH-66 Helicopter," Presented at the American Helicopter Society Aeromechanics Specialist Meeting, Fairfield County, CT, October 1995.
29. Gentry, G. L., Quinto, P. F., Gatlin, G. M., and Applin, Z. T., "The Langley 14- by 22-Foot Subsonic Tunnel: Description, Flow Characteristics, And Guide For Users," NASA TP 3008, Sept. 1990.
30. Gorton, S. A., Poling, D. R., and Dadone, L., "Investigation Of Blade-Vortex Interaction Using Laser Velocimetry And Pressure-Instrumented Rotor Blades," NASA TM 4570, Vol. 1, Jan. 1995.
31. Mace, W. D. Jr., Elliott, J. W., Blancha, B., and Murphy, J., "Comparison Of Frequency Domain And Time Domain Laser Velocimeter Signal Processors," 14th International Congress on Instrumentation in Aerospace Simulation Facilities, Rockville, MD, 1991.
32. Meyers, J. F., Lee, J. W., and Covone, A. A., "Three Component Doppler Global Velocimeter Measurements Of The Flow Above A Delta Wing," 6th International Symposium on Applications of Laser Techniques to Fluid Mechanics, paper 13.2, Lisbon, 1992.
33. Meyers, J. F., Usry, J. W., and Miller, L. S., "Assessing The Capability Of Doppler Global Velocimetry To Measure Vortical Flow Fields," *Journal of Aerospace Engineering*, Vol. 208, (G), pp. 99-105, 1994.
34. Meyers, J. F., "Development Of Doppler Global Velocimetry For Wind Tunnel Testing," AIAA 18th Aerospace Ground Testing Conference, Paper 94-191490, Colorado Springs, CO, 1994.
35. Stepniewski, W. Z., and Keys, C. N., *Rotary-Wing Aerodynamics*. Dover Publications, Inc., New York, 1984, p. 64.

Table 1. Description of rotor blades.

Airfoil sections		Number of blades	4
23.7-percent radius	VR-12	Pitch axis, percent of chord	25
84.6-percent radius	VR-12	Radius, in	34.55
91.8-percent radius	SSC-A09	Solidity, thrust-weighted	0.07866
100-percent radius	SSC-A09	Tip sweep angle (of 1/4 chord), deg	30
Chord, in		Tip sweep begins, in	31.7
23.7-percent radius	2.25	Twist, deg	
74.3-percent radius	2.25	0 percent radius	0
91.8-percent radius	2.25	23.7-percent radius	0
100-percent radius	1.35	74.3-percent radius	-6.6
Cutout, in	8.2	84.6-percent radius	-7.6
Flapping hinge offset, in	2.0	91.8-percent radius	-9.5
Lag hinge offset, in	2.0	100-percent radius	-9.5

Table 2. Flight Conditions

Variable	BL	TF	MR	MRTF	Horizontal Tail			
Advance ratio	NA	NA	0.076	0.076	0.055	0.076	0.102	0.15
Collective, deg	NA	NA	7.1	7.4	11.0	10.1	8.9	7.5
Density, slug/ft^3	.00249	.00243	.00242	.00241	.00236	.00237	.00236	.00235
Fuselage angle of attack, deg	-0.67	-0.63	-0.72	-0.74	-0.89	-0.96	-0.86	-0.86
Freestream velocity, ft/sec	54.9	55.0	55.2	55.2	40.0	54.7	73.8	108.9
Freestream velocity, knots	32.6	32.6	32.7	32.7	23.7	32.4	43.7	64.5
Fuselage yawing moment, in-lb	-25.7	-342.8	-75.0	-641.9	-473.4	-631.3	-815.5	-781.4
Lateral cyclic, deg	NA	NA	1.1	1.1	1.2	1.3	1.9	2.5
Longitudinal cyclic, deg	NA	NA	-3.0	-3.0	-2.8	-3.0	-3.2	-2.7
Rotor drag, lb	NA	NA	2.1	1.7	0.6	2.8	2.6	3.3
Rotor lift, lbs	NA	NA	170.0	169.0	230.5	228.9	229.4	228.8
Rotor rpm	NA	NA	2401	2400	2400	2399	2402	2401
Rotor shaft angle, deg	NA	NA	-0.60	-0.63	-0.66	-0.61	-0.61	-0.61
Rotor thrust coefficient	NA	NA	.00512	.00512	.00714	.00706	.00707	.00709
Rotor yawing moment, in-lb	NA	NA	330.3	324.4	540.3	497.2	421.8	310.0
Tail fan rpm	NA	5007	NA	5394	4860	5197	6262	5435

Table 3. Non-linear Interference Velocities

Location (measured from center of fan)	MRTF - (MR + TF), ft/sec			Velocity, % MRTF		
	u	v	w	u	v	w
1 inch upstream 0.7 inch up	-3.5	2.9	-9.1	-4.0	-18.8	11.6
1 inch downstream 0.7 inch up	-6.7	0.9	-7.8	-8.3	-4.6	10.0
1 inch upstream 2.7 inch up	-3.9	6.9	-6.2	-4.7	-34.8	7.5
1 inch downstream 2.7 inch up	-6.9	5.2	-15.9	-9.3	-23.3	19.9